AIP | Physics of Fluids

Numerical study of the onset of thermosolutal convection in rotating spherical shells

Marta Net, Ferran Garcia, and Juan Sánchez

Citation: Phys. Fluids **24**, 064101 (2012); doi: 10.1063/1.4723865
View online: http://dx.doi.org/10.1063/1.4723865
View Table of Contents: http://pof.aip.org/resource/1/PHFLE6/v24/i6
Published by the American Institute of Physics.

Numerical study of the onset of thermosolutal convection in rotating spherical shells

Marta Net, Ferran Garcia, and Juan Sánchez
Departament de Física Aplicada Universitat Politècnica de Catalunya, Jordi Girona Salgado 1–3, Campus Nord, Mòdul B4, 08034 Barcelona, Spain

(Received 16 July 2011; accepted 16 May 2012; published online 1 June 2012)

The influence of an externally enforced compositional gradient on the onset of convection of a mixture of two components in a rotating fluid spherical shell is studied for Ekman numbers $E = 10^{-3}$ and $E = 10^{-6}$, Prandtl numbers $\sigma = 0.1, 0.001$, Lewis numbers $\tau = 0.01, 0.1, 0.8$, and radius ratio $\eta = 0.35$. The Boussinesq approximation of the governing equations is derived by taking the denser component of the mixture for the equation of the concentration. Differential and internal heating, an external compositional gradient, and the Soret and Dufour effects are included in the model. By neglecting these two last effects, and by considering only differential heating, it is found that the critical thermal Rayleigh number R_e^c depends strongly on the direction of the compositional gradient. The results are compared with those obtained previously for pure fluids of the same σ. The influence of the mixture becomes significant when the compositional Rayleigh number R_c is at least of the same order of magnitude as the known R_e^c computed without mixture. For positive and sufficiently large compositional gradients, R_e^c decreases and changes sign, indicating that the compositional convection becomes the main source of instability. Then the critical wave number m_c decreases, and the drifting waves slow down drastically giving rise to an almost stationary pattern of convection. Negative gradients delay the onset of convection and determine a substantial increase of m_c and ω_c for R_c sufficiently high. Potential laws are obtained numerically from the dependence of R_e^c and of the critical frequency ω_c on R_c, for the moderate and small Ekman numbers explored. © *2012 American Institute of Physics*. [http://dx.doi.org/10.1063/1.4723865]

I. INTRODUCTION

The understanding of the convection in binary fluid spherical shells is fundamental in astrophysics, geophysics, and magnetohydrodynamics. For instance, the Earth's magnetic field is generated in its interior by convection driven by thermal and compositional buoyancy. In addition to the secular cooling of the core, a non-negligible contribution to the energy output of the core is supplied by the latent heat released during crystallization of the inner core, and by the gravitational energy released as the fluid, enriched in light elements by crystallization of the inner core, rises.[1] On the other hand, the thermal convection in the major planets and stars is also affected by the composition of its atmospheres and deep layers. For instance, stars with less than 1.1 solar masses, and belonging to the lower main sequence, possess an inner radiative zone and an outer convective region, mainly of hydrogen, below the photosphere.[2]

The Boussinesq approximation of the onset of convection of a pure fluid subject to radial gravity in rotating spherical shells is well studied (see Refs. 3–9 among many others). According to Ref. 10 when the first bifurcation is of Hopf type and breaks the axisymmetry of the conduction state it gives rise to waves travelling in the azimuthal direction. With $\eta = 0.35$ and differential heating, which are the conditions used in this study, and for $\sigma = 0.1$ at moderate E, the preferred pattern of convection fills the shell up to high latitudes, keeping the polar regions almost motionless, but at low E it is of columnar type, confined near the inner boundary. In contrast with internal heating, at $\sigma = 0.001$ and very low E, the modes of convection remain attached to the outer spherical surface,

and confined near the equator.[11] It is important to stress that the differences are not only due to the Prandtl number but also to the type of heating. We have checked that for the latter σ, the preferred modes can be antisymmetric with differential heating. For instance, this happens for $E = 10^{-6}$, and then the kinetic energy density is concentrated in the polar regions. The above mentioned modes are dynamically controlled by the Coriolis force, and it will be shown that, at least with differential heating, they are also preferred in double-diffusive convection at low E provided that $|R_c| \lesssim |R_e^c|$.

Very few is known about the threshold of thermosolutal convection with a mixture of two components in spherical geometry. By taking into account that heat diffuses much faster than chemical elements, the small gap rotating cylindrical annulus configuration was used in Ref. 12 to demonstrate theoretically that the interaction of two components can facilitate the convection driven by buoyancy. In Ref. 13, an almost adiabatic model of convection was employed to retain the pressure effect through the layer by solving the entropy equation instead of that of the temperature. The approximation is based on a seminal work,[14] in which a full set of non-Boussinesq equations governing the thermal convection in thick planetary interiors was derived. This approach allows to study compositional convection by assuming that the inner power flux is mainly compositional. They analyzed the neutral stability of the compositional-thermal turbulent geo-convection with $\sigma = 1$ and opposite driving gradients. The relative importance of the thermal and compositional gradients may change with the size of the cores along the history of the planets.[15] So, according to Ref. 14 the preceding situation might occur in some terrestrial planets in their final evolutionary stages.

Since 1990s,[16] there is a renewed interest in the contribution of the composition in sustaining a dynamo. Nonlinear simulations of the geodynamo phenomena driven by thermal and compositional convection, and a lot of theoretical papers, have been carried out to help to understand its role in the generation of magnetic fields. In Ref. 17, the anelastic approximation for a fluid binary alloy was used to compute an approximation of the Earth's magnetic field between reversals, assuming the same diffusivities for the entropy and the composition.

Recently, the influence of the driving mechanisms on the convective flow patterns, and the mean and global physical quantities was explored in Ref. 18 by considering the join action of thermal and compositional destabilizing sources, and the same boundary conditions for Θ and Σ. They found that the flow changes from being close to geostrophic for pure thermal driving to being rather non-geostrophic and of smaller scale for purely compositional driving. In this last case, the zonal flows and helicity are dominated by a polar compositional plume.

A model of double-diffusive convection with different diffusivities ($\tau = 0.1$), and realistic boundary conditions, is used in Ref. 19 to analyze the scenario of a deep dynamo below a stable layer in Mercury's core, and to compare the magnetic field intensity at the surface of the planet with those found previously by using an equivalent model but with the codensity formulation. In both studies, the authors consider a core that may be thermally stable from the core-mantle boundary to a substantial depth. This type of stratification seems to be the reason for the weakness of Mercury's magnetic field. They conclude that even low sulphur concentrations give rise to differences with the codensity model that are not negligible.

The main aim of this work is to study the influence of an externally enforced compositional gradient on the onset of convection of a mixture of two components in a rotating fluid spherical shell. Two possible situations are considered. In the first, a stabilizing compositional gradient is imposed. This type of thermosolutal convection should predominate, for instance, in main-sequence stars having a heated helium-rich core surrounded mainly by lighter hydrogen. In the second, the compositional gradient is destabilizing. Such situation occurs, for instance, in the Earth's core where the solidification of dense metallic iron-nickel crystals on the inner core and the release of light components, such as silicon, drives the convection in the outer core more efficiently than thermal gradients.[20,21]

The remainder of the paper is organized as follows. In Sec. II, we extend the classical Boussinesq approximation to the equations for double-diffusive convection in a rotating spherical geometry. The numerical treatment of the linearized equations is also outlined. The accuracy of the numerical results is estimated in Sec. III. In Sec. IV, the neutral stability curves for fixed $\sigma = 0.1$, $\eta = 0.35$, several E and τ numbers, and the preferred modes of convection are analyzed. This Prandtl number was selected following Ref. 22 because it is the last estimated value for the Earth's outer core. For

the sake of completeness, and taking into account that it is poorly determined, the same study is done in Sec. V for $\sigma = 0.001$, $\eta = 0.35$, and $E = 10^{-3}$. The paper concludes with a summary of the results obtained.

II. MATHEMATICAL FORMULATION

Although we seek to study the influence of a mixture of two fluids in the onset of convection generated by external compositional and temperature gradients in a rotating spherical shell, general equations are derived for a binary mixture of fluids heated either internally and/or differentially, and the Soret and Dufour effects[23] are included in the general formulation.

The spherical shell considered is rotating about an axis of symmetry with constant angular velocity $\mathbf{\Omega} = \Omega\mathbf{k}$, and subject to a radial gravity $\mathbf{g} = -\gamma\mathbf{r}$, where γ is a constant, and $\mathbf{r}$ the position vector. The gap width is $d = r_o - r_i$, where r_i and r_o are the inner and outer radii, respectively.

The mass conservation, linear momentum, energy, and concentration for the denser component equations are written in the rotating frame of reference. To take into account the Soret and the Dufour effects in the formulation of the problem, and following Refs. 24 and 25 the flux densities of diffusion of components and heat are written as

$$\mathbf{J}_c = -\rho D\left(\nabla C + \frac{K_T}{T}\nabla T + \frac{K_p}{p}\nabla p\right) \quad \text{and} \tag{1}$$

$$\mathbf{J}_h = \left(K_T\left(\frac{\partial\mu}{\partial C}\right)_{p,T} - T\left(\frac{\partial\mu}{\partial T}\right)_{p,C} + \mu\right)\mathbf{J}_c - K\nabla T, \tag{2}$$

respectively. In the above expressions, ρ is the density of the mixture, D the diffusion coefficient, K_T the thermal diffusion ratio, K the thermal conductivity, K_p the barodiffusion ratio, and μ the chemical potential. However, since we will suppose that the motion of the fluid is caused by temperature and compositional gradients maintained through the boundaries, we will neglect the term in ∇p from $\mathbf{J}_c$.[24]

The equations are derived by extending the Boussinesq approximation to the equation for the concentration. Accordingly, the density in the buoyancy force is taken as

$$\rho = \overline{\rho}(1 - \alpha(T - \overline{T}) + \beta(C - \overline{C})), \tag{3}$$

α and β being the thermal and the compositional expansion coefficients, respectively, measured at the volume-averaged temperature $\overline{T}$ and concentration $\overline{C}$ for which the mean density is $\overline{\rho}$. They are defined as

$$\alpha = -\frac{1}{\overline{\rho}}\left(\frac{\partial\rho}{\partial T}\right)_{T=\overline{T}} \quad \text{and} \quad \beta = \frac{1}{\overline{\rho}}\left(\frac{\partial\rho}{\partial C}\right)_{C=\overline{C}}. \tag{4}$$

We will suppose that the dependence of ρ with p is very small,[25] and consequently will be neglected. Despite this approximation is strictly valid in laboratory conditions, and it is not fulfilled in stars and planetary interiors at high non-linear regimes, it supplies a preliminary knowledge of how the composition modifies the convection at onset.

The coefficients of the gradients in $\mathbf{J}_c$ and $\mathbf{J}_h$ are taken constant, all of them averaged in the full domain. Then, the fluxes of heat and mass become proportional to both ∇C and ∇T, giving rise to the Soret and Dufour effects. The first accounts for the generation of mass fluxes due to the existence of temperature gradients. We have checked that when external compositional gradients are imposed it gives rise to second order effects (see last paragraph in Sec. IV B). The second accounts for the generation of heat fluxes due to the existence of compositional gradients. This effect is, in any case, very small for liquids.[23]

The nondimensional form of the equations is obtained by using d as length, $\nu^2/\gamma\alpha d^4$ as temperature, $\nu^2/\gamma\beta d^4$ as concentration, and d^2/ν as time scales, where ν is the kinematic viscosity. They are

$$\nabla \cdot \mathbf{v} = 0, \tag{5}$$

$$(\partial_t + \mathbf{v}\cdot\nabla)\mathbf{v} = -\nabla\pi + \nabla^2\mathbf{v} - 2E^{-1}\mathbf{k}\times\mathbf{v} + (T - C)\mathbf{r}, \tag{6}$$

$$\sigma(\partial_t + \mathbf{v}\cdot\nabla)T = (QS^2\tau + 1)\nabla^2 T + QS\tau\nabla^2 C + 3R_i/\sigma, \tag{7}$$

$$\sigma(\partial_t + \mathbf{v}\cdot\nabla)C = \tau(\nabla^2 C + S\nabla^2 T). \tag{8}$$

In the above system, $\Omega^2/\gamma \ll 1$ is considered, as happens in the Earth's outer core or in the major planets, and π contains the constant terms coming from $\rho(T, C)$.

The equations can be written in terms of the perturbation ($\mathbf{v}'$, Θ, Σ) of the velocity, temperature, and concentration fields, ($\mathbf{v}$, T, C), from the basic state ($\mathbf{0}$, $T_c(r)$, $C_c(r)$). By considering perfectly conducting ($T(r_i) = T_i$ and $T(r_o) = T_o$) boundaries and constant concentration ($C(r_i) = C_i$ and $C(r_o) = C_o$) on them

$$T_c(r) = T_0 - \frac{R_i}{2\sigma}r^2 + \left(\frac{R_e - \delta R_i}{\sigma}\right)\frac{\eta}{(1-\eta)^2}\frac{1}{r} \quad \text{and} \tag{9}$$

$$C_c(r) = C_0 + \frac{R_i S}{2\sigma}r^2 + \left(\frac{\delta R_i S + R_c\tau}{\sigma}\right)\frac{\eta}{(1-\eta)^2}\frac{1}{r}. \tag{10}$$

The parameter $\delta = (1+\eta)/2(1-\eta)$ is the mean radius, and $r = ||\mathbf{r}||_2$. Substituting ($\mathbf{0}$, $T_c(r)$, $C_c(r)$) in the system of equations, and dropping the primes, we find

$$\nabla\cdot\mathbf{v} = 0, \tag{11}$$

$$(\partial_t + \mathbf{v}\cdot\nabla)\mathbf{v} = -\nabla\Pi + \nabla^2\mathbf{v} - 2E^{-1}\mathbf{k}\times\mathbf{v} + (\Theta - \Sigma)\mathbf{r}, \tag{12}$$

$$\sigma(\partial_t + \mathbf{v}\cdot\nabla)\Theta = (QS^2\tau + 1)\nabla^2\Theta + QS\tau\nabla^2\Sigma + \left(R_i - (R_i\delta - R_e)\frac{\eta}{(1-\eta)^2}\frac{1}{r^3}\right)\mathbf{r}\cdot\mathbf{v}, \tag{13}$$

$$\sigma(\partial_t + \mathbf{v}\cdot\nabla)\Sigma = \tau(\nabla^2\Sigma + S\nabla^2\Theta) - \left(R_i S - (R_i S\delta + R_c\tau)\frac{\eta}{(1-\eta)^2}\frac{1}{r^3}\right)\mathbf{r}\cdot\mathbf{v}. \tag{14}$$

The nondimensional internal Rayleigh (R_i), external Rayleigh (R_e), compositional Rayleigh (R_c), Ekman (E), Prandtl (σ), Lewis (τ) and Dufour (Q) numbers, and the separation ratio (S) are

$$R_i = \frac{q\gamma\alpha d^6}{3c_p\kappa^2\nu},\quad R_e = \frac{\gamma\alpha\Delta T d^4}{\kappa\nu},\quad R_c = \frac{\gamma\beta\Delta C d^4}{\nu D}, \tag{15}$$

$$E = \frac{\nu}{\Omega d^2},\quad \sigma = \frac{\nu}{\kappa},\quad \tau = \frac{D}{\kappa},\quad S = \frac{\beta K_T}{\alpha\overline{T}}, \tag{16}$$

$$Q = \frac{\overline{T}\alpha^2}{c_p\beta^2}\left(\frac{\partial\mu}{\partial C}\right)_{\overline{p},\overline{T}},\quad \eta = \frac{r_i}{r_o}, \tag{17}$$

κ being the thermal diffusivity, c_p the specific heat at constant pressure, q the rate of heat due to internal sources per unit mass. Notice that in the full formulation of the problem $\Delta T = T_i - T_o$ and $\Delta C = C_i - C_o$ come from the temperature and composition differences imposed at the boundaries.

The set of equations is completed with the boundary conditions for the perturbations. As we have said before, we solve the problem with non-slip, perfectly conducting boundaries ($\mathbf{v} = 0$, $\Theta = 0$). For instance, in the case of the Earth, the latent heat released in the solidification of the inner core is supposed to contribute to maintain a constant temperature in the inner boundary. For the concentration, we impose $\Sigma = 0$, i.e., fluxes of the separated components of the mixture through the boundaries are allowed. In fact, since the external part of the shell remain stably stratified even for supercritical Rayleigh numbers, a change in the outer boundary condition introduces minor variations in the flow velocity.[19]

The large number of parameters in the equations determines the need of restricting the range of validity of the computations by doing some approximations. From now on we will always consider

differential heating, namely, $R_i = 0$ and $Q = 0$. Moreover, $S \neq 0$ will be taken only for two sets of parameters in order to compare the solution with $S = 0$.

The linear modes are computed with the method described in Ref. 8. The solenoidal velocity field is written in terms of toroidal Ψ and poloidal Φ potentials

$$\mathbf{v} = \boldsymbol{\nabla} \times (\Psi \mathbf{r}) + \boldsymbol{\nabla} \times \boldsymbol{\nabla} \times (\Phi \mathbf{r}), \tag{18}$$

and the linearized equations for both potentials are obtained by applying the operators $\mathbf{r} \cdot \nabla \times$ and $\mathbf{r} \cdot \nabla \times \nabla \times$ to the momentum equation. Then Eqs. (11)–(14) become

$$(\partial_t - \nabla^2) L_2 \Psi = 2E^{-1} (\partial_\varphi \Psi - Q_3 \Phi), \tag{19}$$

$$(\partial_t - \nabla^2) L_2 \nabla^2 \Phi = 2E^{-1} (\partial_\varphi \nabla^2 \Phi + Q_3 \Psi) - L_2(\Theta - \Sigma), \tag{20}$$

$$(\sigma \partial_t - \nabla^2)\Theta = R_e \frac{\eta}{(1-\eta)^2} \frac{1}{r^3} L_2 \Phi, \tag{21}$$

$$(\sigma \partial_t - \tau \nabla^2)\Sigma = S\tau \nabla^2 \Theta + R_c \tau \frac{\eta}{(1-\eta)^2} \frac{1}{r^3} L_2 \Phi. \tag{22}$$

The operators L_2 and Q_3 are defined by $L_2 \equiv -r^2\nabla^2 + \partial_r(r^2\partial_r)$, $Q_3 \equiv r\cos\theta\nabla^2 - (L_2 + r\partial_r)(\cos\theta\partial_r - r^{-1}\sin\theta\partial_\theta)$, (r, θ, φ) being the spherical coordinates, with θ measuring the colatitude.

The boundary conditions on both sides of the shell are, in terms of the potentials,

$$\Phi = \partial_r \Phi = \Psi = \Theta = \Sigma = 0 \quad \text{on} \quad r_i, r_o. \tag{23}$$

The equations for $X = (\Phi, \Psi, \Theta, \Sigma)$ are solved by expanding the eigenmodes in spherical harmonic series up to degree L, namely,

$$X(r, \theta, \varphi, t) = \sum_{l=0}^{L} \sum_{m=-l}^{l} X_l^m(r, t) Y_l^m(\theta, \varphi), \tag{24}$$

with $Y_l^m(\theta, \varphi) = \tilde{P}_l^m(\cos\theta) e^{im\varphi}$, and $\tilde{P}_l^m$ being the normalized associated Legendre functions of degree l and order m defined as

$$\tilde{P}_l^m(\cos\theta) = \sqrt{\frac{2l+1}{2} \frac{(l-m)!}{(l+m)!}} P_l^m(\cos\theta), \quad \text{for} \quad l \geq 0 \quad \text{and} \quad 0 \leq m \leq l, \tag{25}$$

$P_l^m(\cos\theta)$ being the associated Legendre functions, and $\tilde{P}_l^{-m}(\cos\theta) = \tilde{P}_l^m(\cos\theta)$. In the radial direction, a collocation method on a Gauss-Lobatto mesh of N points is employed.

III. ACCURACY OF THE RESULTS

The onset of thermosolutal convection for both $R_c < 0$ and $R_c > 0$ is studied. Notice that this means $\Delta C = C(r_i) - C(r_o) < 0$ and $\Delta C = C(r_i) - C(r_o) > 0$. As said before, because (19)–(23) are written for the denser component, the first situation applies to the present-day Earth's outer core, and the second would correspond to some stars or major planets, where the heavy components such as helium could be placed in the deeper layers.

In general, a higher concentration of the denser component of the mixture near the outer boundary than at the inner gives rises to a destabilizing compositional gradient that reinforce the destabilizing temperature gradient. So, for high enough compositional gradients the onset of convection could take place even with stabilizing temperature gradients, i.e., with negative thermal Rayleigh numbers. In contrast, the highest concentration of the denser component in the interior implies a stabilizing compositional gradient that leads to an increase of the modulus of the critical temperature gradient to trigger the convection, i.e., higher $R_e^c > 0$ values than those of a pure fluid.

In order to check the code, the critical parameters for the onset of convection of a pure and three binary fluids of $\sigma = 0.1$, filling a spherical shell of $\eta = 0.35$, have been compared. Some of them

TABLE I. Comparison of the critical values for a pure and two binary fluids of $\sigma = 0.1$, $S = 0$, and different values of E, R_c, and τ.

E	τ	R_c	m_c	${R_e}^c$	$-\omega_c$
10^{-3}	0	0	3	2.088×10^4	1.013×10^2
10^{-3}	0.01	10^4	3	2.085×10^4	1.025×10^2
10^{-3}	0.01	-10^4	3	2.091×10^4	1.000×10^2
10^{-3}	0.1	10^4	3	2.121×10^4	1.128×10^2
10^{-3}	0.1	-10^4	3	2.039×10^4	8.754×10^1
10^{-6}	0	0	23	3.324×10^7	1.101×10^4
10^{-6}	0.01	10^6	23	3.318×10^7	1.100×10^4
10^{-6}	0.1	10^6	23	3.323×10^7	1.102×10^4
10^{-6}	0.1	-10^6	23	3.313×10^7	1.097×10^4

are shown in Table I. Like for the pure fluid the bifurcation from the conduction state gives rise to an azimuthal drifting wave. The results of the rows with $R_c = 0$ have been computed with the same code as the others setting $S = 0$, and checked to agree with those computed with an older[8] code written for the pure fluid. For $\tau \neq 0$, and the values of R_c selected, the eigenvalues and eigenmodes do not differ very much from those obtained for $R_c = 0$ because, as it will be seen later on, for each τ a minimum value of R_c is needed to observe important changes in the results. In addition, we have compared the ratio of the pure compositional, R_c^c, and thermal, R_e^c, critical Rayleigh numbers with those found in Ref. 18 for $\sigma = 0.3$, $\tau = 0.1$, and $E = 10^{-3}$ by using a nonlinear time evolution code. In our case, with the same parameters and $m_c = 4$, we obtain $R_e^c = 2.76 \times 10^4$ with $\omega_c = -58.72$ and $R_c^c = -4.10 \times 10^4$ with $\omega_c = -7.263$. Taking into account the relation between the Rayleigh numbers of Ref. 18 (R_e^{Br} and R_c^{Br}) and those defined here, i.e., $R_e^{Br} = (1-\eta)^{-1} R_e$ and $R_c^{Br} = -(1-\eta)^{-1} R_c$, we got $(R_e^{Br})_c = 4.25 \times 10^4$ and $(R_c^{Br})_c = 6.30 \times 10^4$ for the critical values, which agree very well with their values (4.21×10^4 and 6.10×10^4, respectively). The factor is $|R_c^c / R_e^c| = 1.48$, which is quite close to theirs (1.45), confirming that the compositional convection is triggered at higher critical values than the thermal. The ratio between the corresponding frequencies is 0.135, so pure thermal waves drift, at onset, 7.4 times faster than the compositional.

For $\sigma = 0.1$, the solutions are computed by using 50 radial points and spherical harmonics of maximal degree 80 when $E = 10^{-3}$, and 60 radial points and spherical harmonics of maximal degree 100 for $m \leq 24$, 120 for $25 < m < 31$ and 150 for $m \geq 31$ when $E = 10^{-6}$. With these resolutions the maximal relative errors are below 2% for R_e^c, and 0.6% for ω_c. Some values of R_e^c and ω_c with the corresponding relative errors are shown in Table II. The latter are calculated by comparing the solutions obtained with $(N, L) = (50, 80)$, $(60, 100)$, and $(60, 120)$ with those obtained with $(N, L) = (60, 100)$, $(60, 120)$, and $(60, 150)$, respectively. We have selected solutions with large wave numbers because they have the larger errors. Finally, we include Table III showing the convergence of solutions of wave number $m = 23$ and 33 with $R_c = 10^6$, $\sigma = 0.1$, $\tau = 0.1$, and $E = 10^{-6}$. It makes clear that a resolution of 60 radial points is sufficient for resolving the boundary layer structure in the linear problem.

TABLE II. Values of ${R_e}^c$ and ω_c, and their corresponding relative errors $\varepsilon_{Re}(\%)$, $\varepsilon_\omega(\%)$ for $\sigma = 0.1$, $S = 0$ and different values of E, m, τ, and R_c.

E	m	τ	$R_c \times 10^{-9}$	${R_e}^c \times 10^{-8}$	$\varepsilon_{R_e^c}$	$-\omega_c \times 10^{-4}$	ε_{ω_c}
10^{-3}	15	0.1	0.95	0.211	0.0001	2.813	0.002
10^{-6}	26	0.8	1.0	7.52	0.02	3.009	0.01
10^{-6}	33	0.1	2.0	0.766	0.3	3.499	0.06
10^{-6}	31	0.01	4.5	0.419	0.4	2.109	0.005
10^{-6}	33	0.1	−0.1	0.202	1.7	0.441	0.59

TABLE III. Convergence of $R_e{}^c$ and ω_c for $E = 10^{-6}$, $\tau = 0.1$, $\sigma = 0.1$, and $R_c = 10^6$ and -10^8 for $m = 23$ and $m = 33$, respectively.

N	L	m	$R_e{}^c \times 10^{-7}$	$-\omega_c \times 10^{-4}$
50	100	23	3.3751	1.0957
60	100	23	3.3229	1.1020
70	100	23	3.2970	1.1045
80	100	23	3.2937	1.1048
60	120	23	3.3290	1.1034
70	120	23	3.3032	1.1059
80	100	33	1.2829	0.3498
60	120	33	2.0228	0.4411
70	120	33	1.9846	0.4435
60	150	33	2.0560	0.4437
80	150	33	2.0122	0.4463

For $\sigma = 0.001$, we have employed $(N, L) = (50, 80)$ for low R_c values, and (60, 100) for the largest.

IV. PRANDTL NUMBER $\sigma = 0.1$

A. Positive compositional gradients

In this case ($\Delta C < 0$ and $R_c < 0$), all the calculations are done with $S = 0$.

Figure 1, computed for $\tau = 0.1$, shows the dependence of the critical thermal Rayleigh number for a fixed wave number m, $(R_e^m)_c$, and the associated precession frequency, ω_c^m, for $m = 1, \ldots, 7$ and moderate $E = 10^{-3}$. The critical Rayleigh number R_e^c corresponds to the envelope of these curves, which gives the minimum value. Negative precession frequencies mean that the waves travel in the prograde direction with phase speed $c_m = -\omega_c^m/m$. Axisymmetric solutions are never preferred.

From $R_c = 0$ to -10^4, the onset of convection for the binary fluid does not change significantly with respect to that of a pure fluid, i.e., the critical parameters differ very little from those shown in Table I for $R_c = 0$.

From approximately $R_c = -10^4$, $(R_e^3)_c$ decreases, and the preferred wave number is still $m_c = 3$. At $R_c = -1.34 \times 10^4$ it changes to $m_c = 4$, $m_c = 5$, and again $m_c = 4$, denoting that the influence of the compositional gradient starts to be as important as that of the temperature gradient. From $R_c = -3.64 \times 10^4$, R_e^c becomes negative indicating that the compositional convection is possible even with $T_i < T_o$. When this happens the precession frequencies ω_c^m start to increase abruptly and tend asymptotically to zero as $-R_c$ increases. The moderate increase of m_c, while the temperature gradient is destabilizing, is in agreement with the results obtained in Ref. 18 for $E = 10^{-3}$, $\tau = 0.1$, and $\sigma = 0.3$, which are very close to the parameters used here. From fully nonlinear calculations they observed the increase in m_c when the convection changes from mainly thermal to mainly compositional (mainly meaning 80% of their combined viscous Rayleigh number) (see Fig. 5 of Ref. 18).

Figure 1(c) shows the asymptotic dependence of R_e^c and ω_c in logarithmic scale. An almost inversely proportional dependence of $-\omega_c$ and an almost linear dependence of $-R_e^c$ with $-R_c$ are found. To be more precise, $R_e^c = -0.24(-R_c)^{1.104}$ and $\omega_c = -4.94 \times 10^5(-R_c)^{-0.983}$, with relative errors lower than 1.5% for R_e^c and ω_c. Unless new bounds of error be specified, these are valid for any asymptotic fitting given along the paper. In this regime, the critical wave number is $m_c = 3$.

The extension of the range of Figs. 1(a) and 1(b) to the left gives asymptotic curves to $R_e^c = 2.088 \times 10^4$ and $\omega_c = -101.3$, respectively, for $m = 3$. The differences between the eigenfunctions in both asymptotic regimes will be commented later.

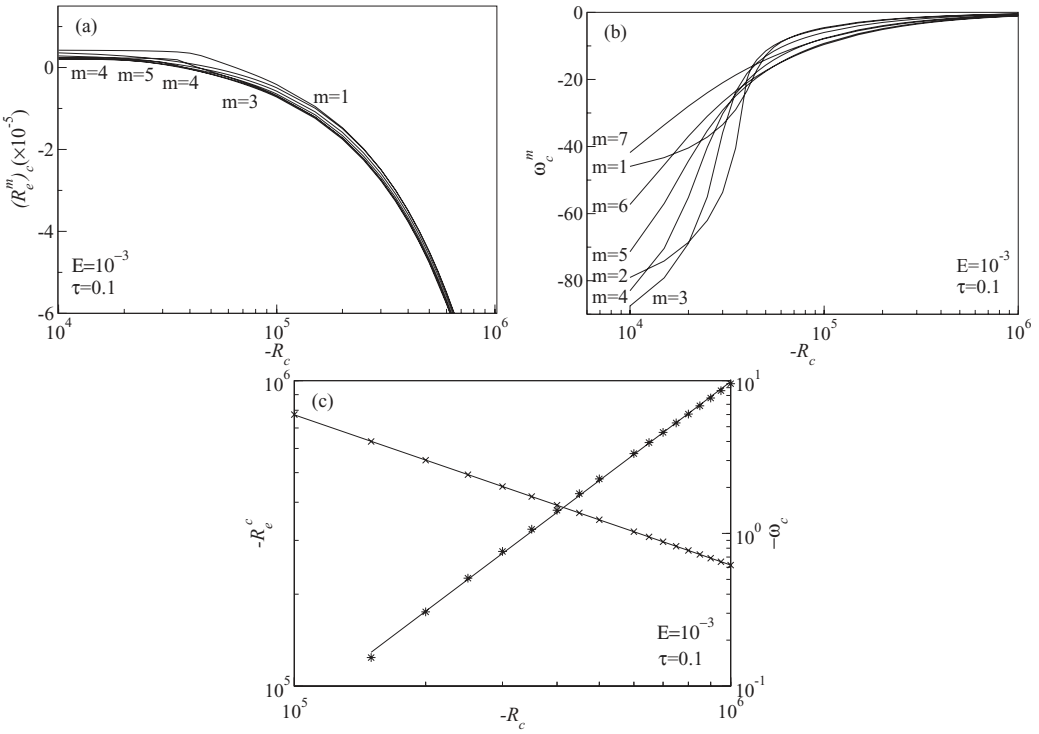

FIG. 1. (a) The critical thermal Rayleigh number $(R_e^m)_c$, (b) the critical precession frequency ω_c^m, for each critical mode of azimuthal wavenumber $m = 1, \ldots, 7$, and (c) the asymptotic law for the critical thermal Rayleigh number $-R_e^c$ ($\times$), and precession frequency $-\omega_c$ ($*$), all of them plotted versus the compositional Rayleigh number $-R_c$ for $E = 10^{-3}$ and $\tau = 0.1$.

In Fig. 2, the same curves as for the preceding parameters can be seen for $\tau = 0.01$. In this case, the transition from modes dominated by thermal convection to those dominated by compositional convection is much more clear because the neutral stability curve (envelope) consist of two parts belonging to two different families of curves, the straight and the folded. The interchange takes place at $R_c = -3.11 \times 10^4$ where $R_e^c = 2.10 \times 10^4$ and the precession frequency jumps from $\omega_c = -97.24$ with $m = 3$ to $\omega_c = -3.822$ with $m = 6$. By increasing $-R_c$ the wave number $m = 3$ of the pattern of convection is gradually recovered and ω_c tends to zero. So, for both $\tau = 0.1$ and 0.01 the effect of increasing $-R_c$ is to maintain the value of the preferred wave number and to slow down the wave.

The jumps among curves are better illustrated in Fig. 2(b). For $m \geq 6$, the nearly straight lines of Fig. 2(a) cross those folded below the turning point, and the jump in the drifting frequency is then connected by a vertical straight line. For $m < 6$, the crossings take place above the fold. These points are not determined with high precision, therefore, the two curves are left disconnected in Fig. 2(b).

From Fig. 2(c), the asymptotic power laws for R_e^c and ω_c have been found. The dependences are almost linear and inversely proportional as before, with $R_e^c = -0.35(-R_c)^{1.075}$ and $\omega_c = -6.17 \times 10^4(-R_c)^{-1.006}$, respectively.

Although the neutral stability curves $(R_c, (R_e^m)_c)$ for the two sets of parameters presented so far present important differences, their envelopes (R_c, R_e^c) resemble each other closely, as well as the preferred modes, with a region of low $-R_c$ values dominated by the thermal gradient followed by the region dominated by the compositional gradient. Figures 3 and 4 show the contour plots of three projections of Θ, the kinetic energy density, $|\mathbf{v}|^2$, and Σ for $\tau = 0.01$. The spherical sections (a), (d), and (g) are taken on the spheres passing through the maxima of the functions represented. The plots (b), (e), and (h) are equatorial sections, and the meridional sections (c), (f), and (i) also pass through the maxima. The grey scale is the same for each group of contour plots. For Θ, Σ, and $|\mathbf{v}|^2$, white means positive values, and black negative, except for $|\mathbf{v}|^2$ for which it means zero. When the wave number of the solutions is very high the contour lines are

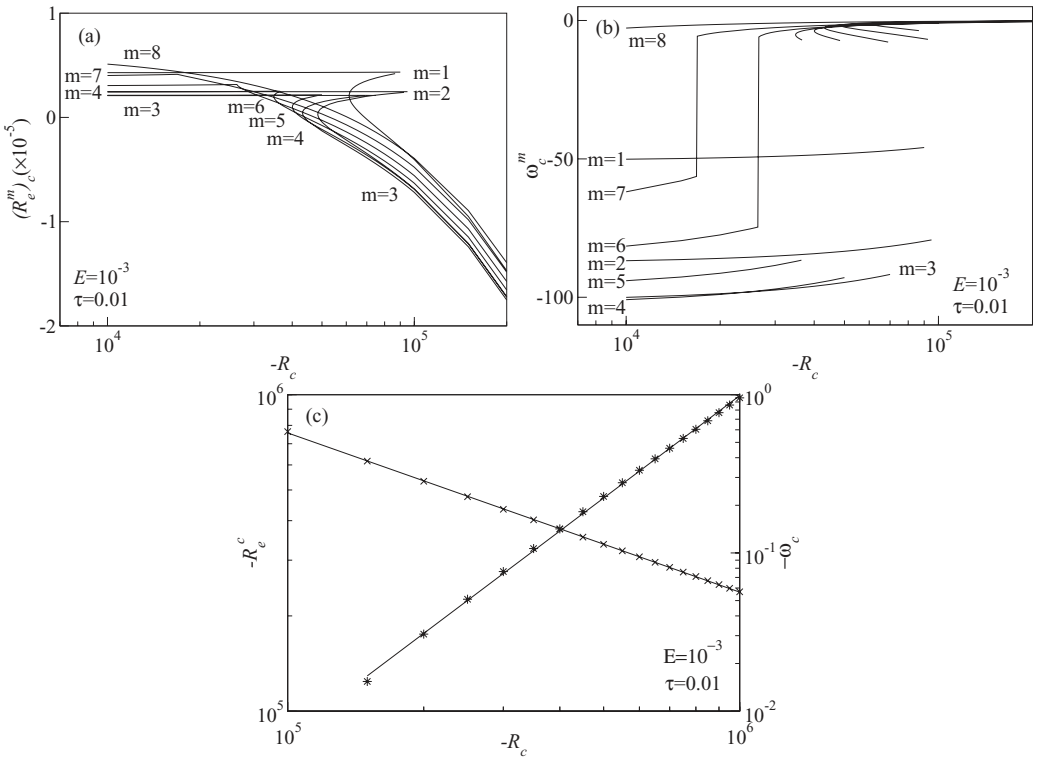

FIG. 2. Idem Fig. 1 for $E = 10^{-3}$ and $\tau = 0.01$.

omitted from the plots since the figures look more clear. These criteria will be kept along the paper.

Figure 3 shows the preferred modes at $R_c = -1.0 \times 10^4$, where the effect of the mixture is weak. Those for Θ and $|\mathbf{v}|^2$ look like those of the pure fluid for the same E. The contour plots of Σ spiral much more and are more confined to the inner boundary than those of Θ. Figure 4 is plotted at $R_c = -7.0 \times 10^{-5}$ in the asymptotic regime of high $-R_c$. The first row of the plots does not differ very much from the preceding case, but the second is nearly indistinguishable from the temperature perturbation of the same figure. This can be explained easily *a posteriori* from Eq. (19) to (23).

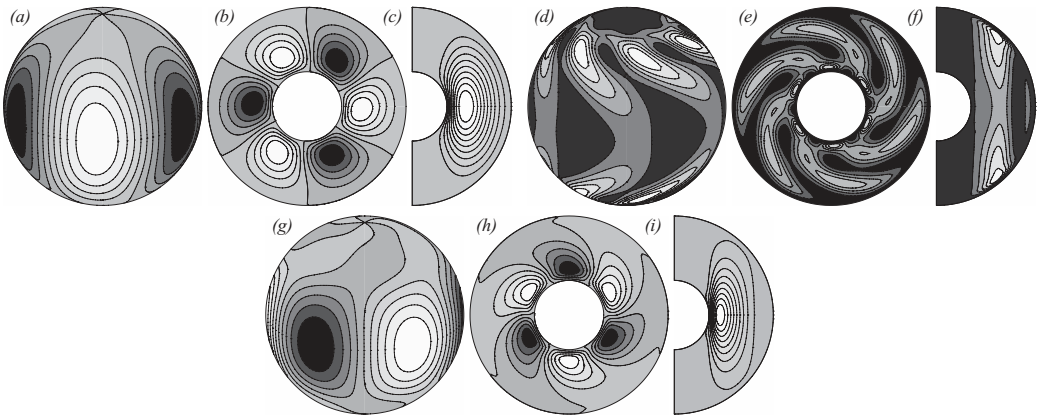

FIG. 3. Contour plots of critical modes. (a)–(c) Temperature perturbation Θ, (d)–(f) kinetic energy density $|\mathbf{v}|^2$, and (g)–(i) concentration perturbation Σ, for $E = 10^{-3}$, $R_c = -1.0 \times 10^4$, $\tau = 0.01$, and $m_c = 3$.

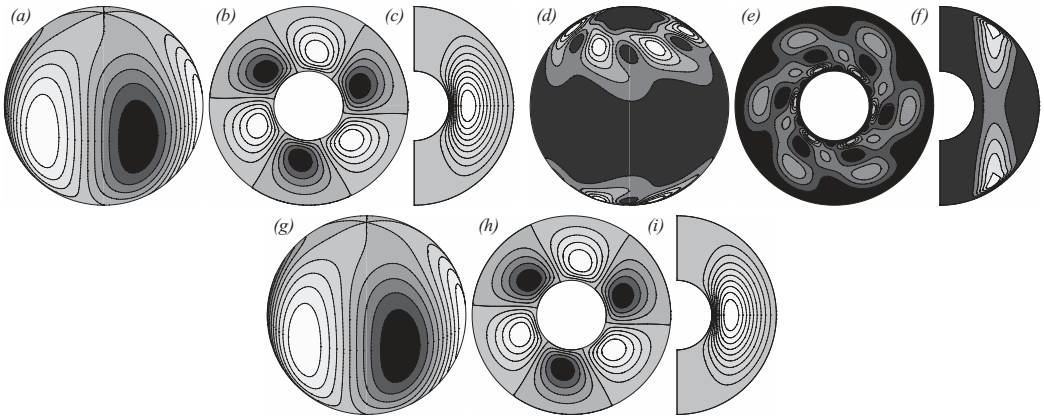

FIG. 4. Idem Fig. 3 for $E = 10^{-3}$, $R_c = -7.0 \times 10^5$, $\tau = 0.01$, and $m_c = 3$.

When $S = 0$, according to Eqs. (21) and (22), the critical modes fulfill

$$\left(i\sigma\omega - \nabla^2\right)\left(\Theta/R_e^c\right) = \frac{\eta}{(1-\eta)^2}\frac{1}{r^3}L_2\Phi, \tag{26}$$

$$\left(i\sigma\omega/\tau - \nabla^2\right)\left(\Sigma/R_c\right) = \frac{\eta}{(1-\eta)^2}\frac{1}{r^3}L_2\Phi. \tag{27}$$

Therefore, as can be seen in Figs. 1(b) and 2(b), if Θ and Σ have the same boundary conditions, in the asymptotic large $-R_c$ limit $\omega_c \to 0$, and Θ/R_e^c and Σ/R_c obey the same equation, so they must be proportional.

The contour plots indicate that E is moderately small because the vortices of convection fill most of the width of the shell and the kinetic energy density is confined at the outer boundary. The main contribution to $|\mathbf{v}|^2$ corresponds to the azimuthal velocity. The radial velocity, which allows to understand easily the dynamics of the vortices, goes almost in (π/m out of) phase with Θ for positive (negative) thermal Rayleigh numbers, respectively. The concentration perturbation is slightly above $\pi/2m$ out of (in) phase with respect to Θ.

The last case considered with positive compositional gradients corresponds to a small Ekman number $E = 10^{-6}$ and $\tau = 0.1$. It is selected because it is known[9] that for these parameters the onset of convection for a pure fluid falls in the rapidly rotating asymptotic limit.

The neutral stability curves for $m = 1, \ldots, 37$ have been computed, and some of them are shown in Fig. 5. Their behavior is more complicated than with moderate E because they can be double folded (for instance, the curve labelled $m = 22$) or even can be the envelope of two folded curves (see, for instance, the $m = 6$ curve inside the fold of $m = 3$ in Fig. 5(a), or in Fig. 5(b)). At $R_c = -1.0 \times 10^7$ the preferred mode is still $m = 23$ as for $R_c = 0$, with critical values $R_e^c = 3.31 \times 10^7$ and $\omega_c = -1.097 \times 10^4$, which are only slightly lower than those of $R_c = 0$ (see Table I).

The effect of increasing $-R_c$ is a slow decrease of $(R_e^m)_c$ and $-\omega_c^m$ up to $R_c = -9.22 \times 10^7$, where $(R_e^m)_c = 2.74 \times 10^7$ and $\omega_c^m = -8.356 \times 10^3$. From this point the compositional gradient starts to be apparent giving rise to a steeper decrease of $(R_e^m)_c$ and $-\omega_c^m$. In this zone, the critical wave number jumps from $m_c = 33$ to 27 passing through 31 and 29. The precession frequency $-\omega_c$ drops from 4.913×10^3 to 2.494×10^3. Below the point $(-R_c, R_e^c) = (1.34 \times 10^8, -2.65 \times 10^7)$ ($R_e^c < -2.65 \times 10^7$), the compositional gradient becomes dominant, and the envelope is made of parts of the folded curves of $m_c = 6$, 2, 3. The wave number jumps to $m_c = 6$ with $\omega_c = -3.350 \times 10^2$, after changes to $m_c = 2$, and at the turning point, located at $R_c \approx -6.51 \times 10^7$, it is already $m_c = 3$ with $\omega_c \approx -20.6$.

Despite E has changed R_e^c and ω_c follow, for large $-R_c$ values, the almost same power laws as for $E = 10^{-3}$. We have found from the envelopes of Figs. 5(a) and 5(b) $R_e^c = -0.49(-R_c)^{1.036}$ and $\omega_c = -1.71 \times 10^9(-R_c)^{-1.054}$. So it seems that these laws do not depend on E. In this case, the relative error for ω_c is less than 2.6%.

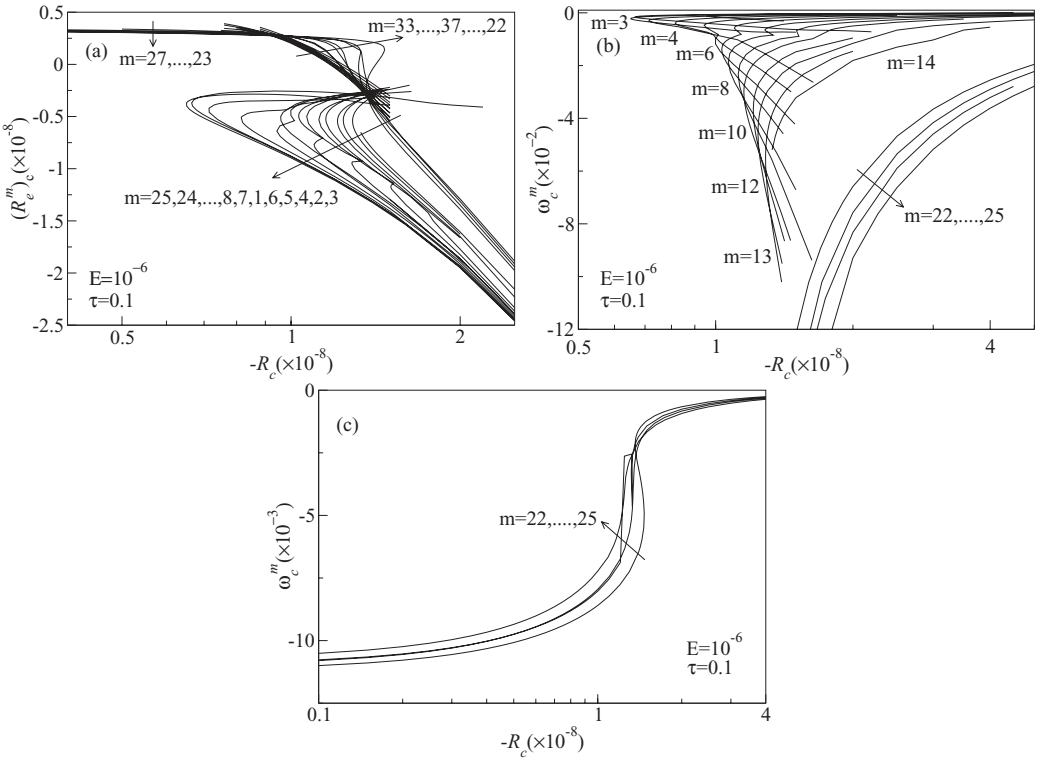

FIG. 5. (a) The critical thermal Rayleigh number $(R_e^m)_c$, (b) the critical precession frequency ω_c^m, for the critical modes labelled in the figure, and (c) enlargement of (b) for the wave numbers $m = 22, \ldots, 25$, all of them plotted versus the compositional Rayleigh number $-R_c$ for $E = 10^{-6}$ and $\tau = 0.1$.

Figure 5(c) shows ω_c^m for $m = 22, \ldots, 25$ in the limit of low $-R_c$ values. The precession frequency of the preferred $m_c = 23$ mode tends to -1.10×10^4 corresponding to the pure fluid.

The preferred modes corresponding to the low $-R_c$ limit are plotted in Fig. 6. In this case, it reflects the low E value selected, with modes attached and confined to the inner boundary, and a very thin columnar kinetic energy density. The contour plots of Σ are like those of Θ but with the phase difference commented before. The radial extend and curvature of the former are a little bit more pronounced.

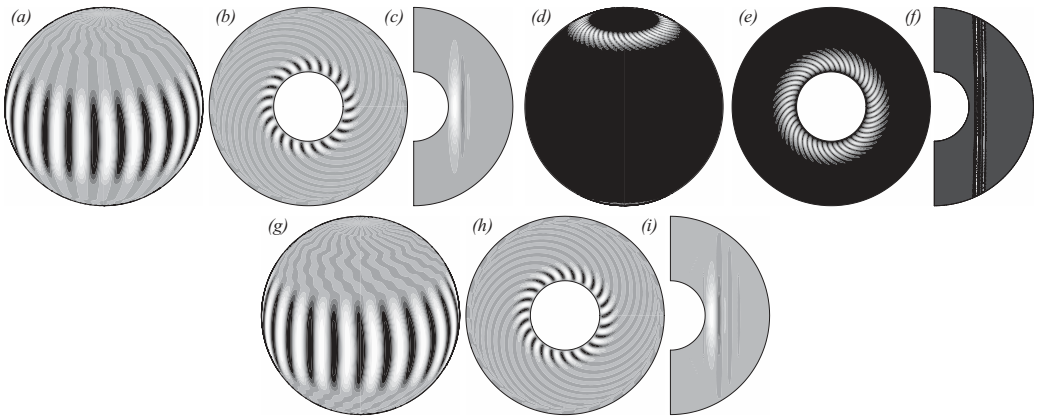

FIG. 6. Idem Fig. 3 for $E = 10^{-6}$, $R_c = -6.0 \times 10^7$, $\tau = 0.1$, and $m_c = 23$.

The contour plots of Θ and Σ in the high $-R_c$ limit (not shown) have $m_c = 3$, and resemble very much to those of Fig. 4. Only the contour plots of $|\mathbf{v}|^2$, which are like those of Fig. 6, exhibit the influence of the low E value, i.e., the large azimuthal velocity of the fluid at high rotation rates Ω or very low viscosities.

The preceding results can also be compared with those obtained theoretically in Ref. 12. For this we have taken into account the dimensions of the Earth's outer core and the estimated relation between the non-dimensional parameters, namely, $R_c^{Bu} = (\tau\delta/d)R_c$, $R_e^{Bu} = (\delta/d)R_e$, and $\eta^* = (4d \tan\chi/h)/E$, where R_c^{Bu} and R_e^{Bu} refer to the compositional and thermal Rayleigh numbers defined in Ref. 12, respectively, $h = 2\sqrt{2d\delta}$ is the height of the annulus, and $\tan\chi$ is the small slope of its lids. There, like here, it is shown that R_e^c is independent of R_c up to values of R_e^c of order R_c. However, there is a discrepancy in the preferred mode of convection. According to Ref. 12 there exists a slow mode of convection of small constant wave number $m_c = 2.22$ preferred when the concentration gradient is weak. In this regime, the torque provided by the compositional buoyancy term can balance the generation of vorticity supplied by the Coriolis force, and then the equations are reduced to those of a cylinder with flat lids for which, with non-slip boundary conditions, the onset of convection gives rise to azimuthal waves drifting very slowly.[26] Both studies agree in the low wave number of the slow waves, but our results show that the slow mode becomes preferred for strong concentration gradients (see Figs. 1, 2, and 5). Consequently, all seems to indicate that at low and moderate $-R_c$ the compositional buoyancy is negligible in front of the thermal buoyancy because of its slow diffusivity, and the dynamics is controlled by the high rotation rates as for the pure fluid. Only at very high $-R_c$ the compositional buoyancy is able to balance the Coriolis force, and to give rise to steady convection against stabilizing temperature gradients.

B. Negative compositional gradients

In this case ($\Delta C > 0$ and $R_c > 0$), the compositional gradient exerts a stabilizing effect, and when it becomes significant the critical thermal Rayleigh number must exceed that of the pure fluid. Unless otherwise stated $S = 0$.

Figure 7 shows the critical parameters R_e^c, $-\omega_c$ and m_c, for $E = 10^{-3}$ and $\tau = 0.1$ and 0.01, versus R_c. Notice that now R_c is positive and the concentration of the denser component is higher near the inner boundary. The range represented starts near the point at which the composition influences the convection. Although up to $R_c = 10^5$, R_e^c is almost constant, ω_c is not. For instance, for $\tau = 0.1$, $\omega_c = -1.127 \times 10^2$ is already more than 11% higher than that given in Table I for $R_c = 0$. We only plot the envelope of the curves because they almost overlap in the large R_c interval presented. As can be seen in the figure, after the noticeable jumps, the slopes of the neutral curves for both τ are almost the same. The asymptotic laws for $\tau = 0.1$, give $R_e^c = 0.07R_c^{0.944}$ and $\omega_c = -0.37R_c^{0.544}$, and for $\tau = 0.01$, $R_e^c = 0.01R_c^{0.907}$ and $\omega_c = -0.11R_c^{0.546}$. While the power for R_e^c is only slightly lower than in the previous case, $-\omega_c$ nearly increases with the square root of R_c.

Although the curves are quite smooth there are a lot of crossings of modes along them, which are shown in Fig. 7(c). To help the reader to follow the preferred wave number, $m_c + 1$ is plotted instead of m_c for $\tau = 0.1$. In addition, the numerical values corresponding to $\tau = 0.01$ are connected by a dashed line. The big jumps in the R_e^c and $-\omega_c$ curves are associated with jumps in m_c, from 4 to 6 for $\tau = 0.1$ and from 4 to 7 for $\tau = 0.01$. The monotonical increase of the wave number at high R_c indicates the onset of prevailing compositional convection, which becomes delayed for low τ.

The preferred modes of convection in the asymptotic regime are shown in Fig. 8 plotted for $\tau = 0.01$. The effect of a very high R_c is to confine the vortices of Θ and Σ near the inner boundary, as for a high rotation rate, but in this case the vertical extent of the vortices is much smaller and they are less spiraled. The kinetic energy density also remains confined near r_i in contrast to Figs. 3 and 4, which are also computed for $E = 10^{-3}$. The larger R_c the shorter the height of the vortices is. Be aware that in Fig. 8 the contributions of the radial and azimuthal velocities to $|\mathbf{v}|^2$ are of the same order of magnitude.

To see what kind of modes could become critical for other parameters, Figs. 9 and 10 depict the preferred eigenfunctions along the $m = 7$ curve of $\tau = 0.1$, which in the range $7.85 \times 10^6 < R_c$

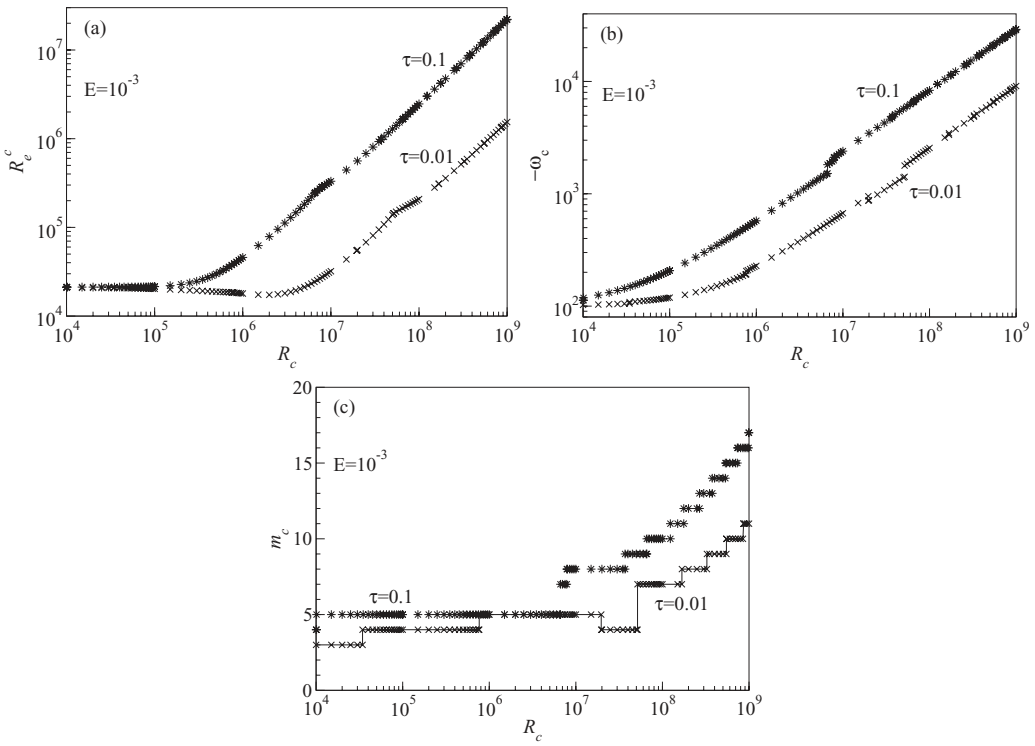

FIG. 7. (a) The critical Rayleigh number R_e^c, (b) the critical precession frequency $-\omega_c$, and (c) the critical wave number m_c for $\tau = 0.01$, and $m_c + 1$ for $\tau = 0.1$, plotted versus R_c for $E = 10^{-3}$.

$< 3.70 \times 10^7$ supplies R_e^c. The contour plots of $\tau = 0.01$ give rise to the same patterns. At $R_c = 10^4$, they are like those of Fig. 3 for any value of τ (as for negative R_c values), i.e., like those of the pure fluid. Despite they are not represented, at low R_c the contour plots of Σ are different from those of Θ. In general, they are more spiraled as for positive compositional gradients (see Fig. 3).

Figure 9 shows three solutions (see the figure caption to know R_c) that belong to an intermediate regime in which the effects of the temperature and compositional gradients are both important. Notice that although the contour plots of Θ initially fill the shell, the velocity field is completely different from that obtained for negative compositional gradients with the same E, now the main contribution to $|\mathbf{v}|^2$ corresponds to the radial velocity. In Figs. 9 and 10, the only wave which travels prograde is that of $R_c = 1.5 \times 10^6$. Figure 10 displays the patterns of convection driven mainly by

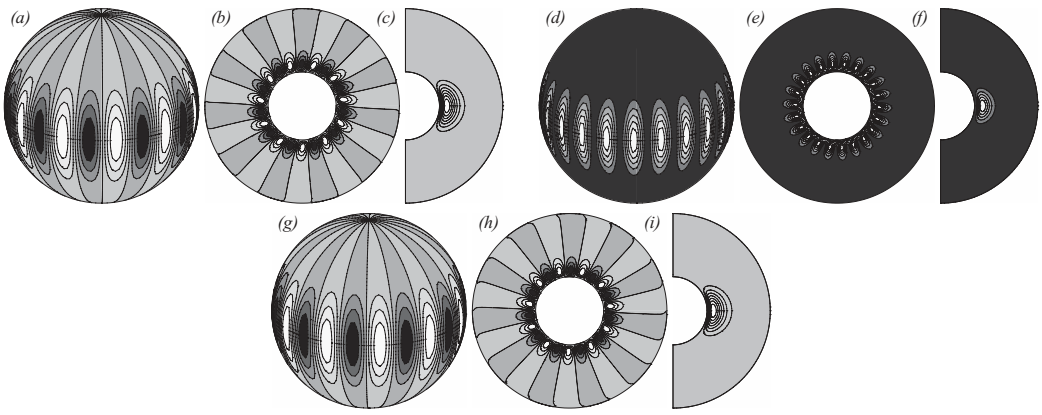

FIG. 8. Idem Fig. 3 for $E = 10^{-3}$, $R_c = 9.0 \times 10^8$, $\tau = 0.01$, and $m_c = 11$.

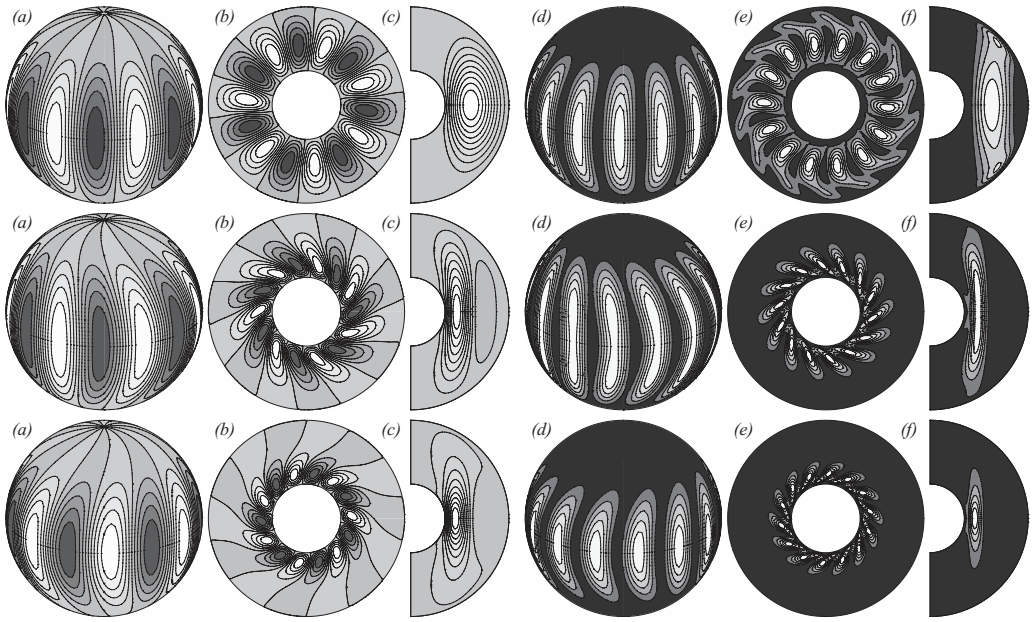

FIG. 9. (a)–(c) Contour plots of Θ, and (d)–(f) of $|\mathbf{v}|^2$ for the preferred eigenfunctions of $m = 7$. From top to bottom, $R_c = 1.5 \times 10^5$, 1.5×10^6, 2.5×10^6. In all cases $E = 10^{-3}$, $\tau = 0.1$, and critical values $R_e = (R_e^7)_c$.

compositional gradients. The first row corresponds to the preferred pattern at high R_c in the curves of Fig. 7 (see also Fig. 8). The next pattern is antisymmetric with respect to the equator, and from $R_c \approx 7.45 \times 10^7$ tesseral modes are selected, namely, modes for which the degree (l) and order (m) of the spherical harmonics of higher amplitude verify $m \neq 0$ and $l - m \neq 0$. In fact, with this definition, the antisymmetric mode is the tesseral mode with $l - m = 1$ and $l = 8$. By increasing R_c this difference increases monotonically for the successive modes. The symmetric patterns have $l - m$ even, and the antisymmetric $l - m$ odd. For instance, the contour plots at $R_c = 5 \times 10^8$, and $R_c = 6 \times 10^8$ have $l - m = 6, 7$, respectively. Notice that for the latter the contour plots on the equator are residual, therefore the grey is uniform.

Nonlinear tesseral patterns of convection were found by Dai *et al.*[27] in the study of hydrothermal convection in a water-saturated porous material of spherical-shell shape. They considered a non-rotating medium, and then there is a multiplicity of steady tesseral states co-existing for the same value of the Rayleigh number.

Finally, Fig. 11 summarizes the results obtained for $\tau = 0.8$, 0.1 and 0.01 with $E = 10^{-6}$. The curves are smooth and show the same tendency as for moderate Ekman numbers (see Fig. 7). The lower τ the stronger must the compositional gradient be to make the mixture effects clear. For high R_c values, R_e^c and ω_c also exhibit a potential law dependence on R_c. The powers are lower than those found for $E = 10^{-3}$. In the range computed we have found, for $\tau = 0.01$, $R_e^c = 5.67 \times 10^6 R_c^{0.089}$ and $\omega_c = -1.73 R_c^{0.418}$ with relative error of 2.8%, for $\tau = 0.1$, $R_e^c = 4.64 R_c^{0.770}$ with relative error of 5.7% and $\omega_c = -0.69 R_c^{0.505}$, and, for $\tau = 0.8$, $R_e^c = 12.2 R_c^{0.866}$ and $\omega_c = -3.57 R_c^{0.435}$ with relative error of 2.6%. Extremely large critical values were also described in Ref. 13 for the threshold of their almost adiabatic model of thermosolutal convection with $\sigma = 1$, when the compositional convection is stabilizing.

In Fig. 11(c), the wave numbers m_c, $m_c - 1$, and $m_c + 1$ are plotted for $\tau = 0.01$, $\tau = 0.8$, and $\tau = 0.1$, respectively. As before the numerical values corresponding to $\tau = 0.01$ are connected by a dashed line. The wave numbers increase from $m = 23$ to $m = 35$ for $\tau = 0.01$, to $m = 33$ for $\tau = 0.1$, and to $m = 25$ for $\tau = 0.8$, although in this case the curve finishes at 10^9 instead of at 10^{10}. Notice that for $\tau = 0.1$ and 0.01 all the preferred eigenfunctions have odd azimuthal wave numbers. As a sample, one of them is shown in Fig. 12 for $\tau = 0.01$. Since $E = 10^{-6}$ is very low, the contour

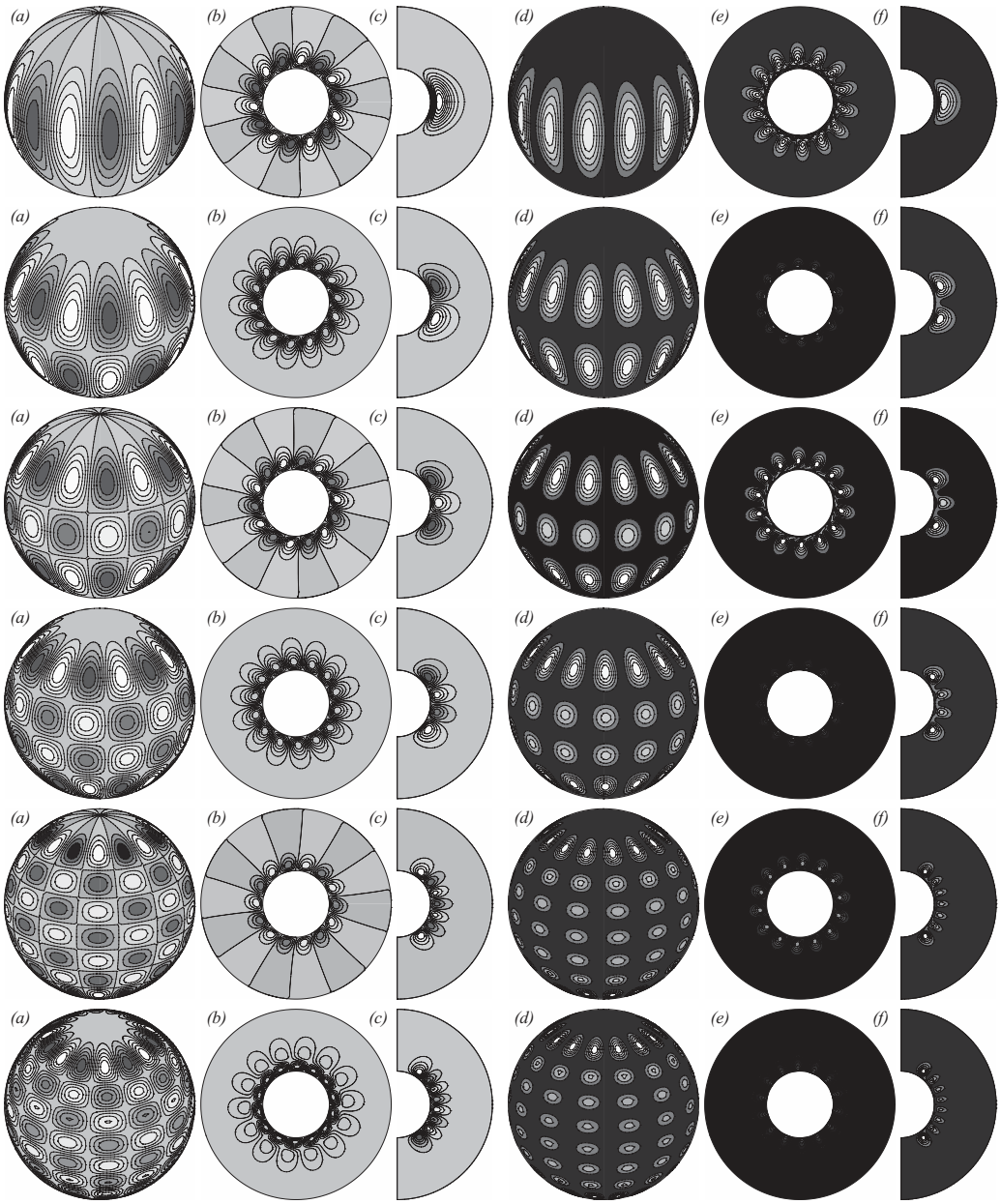

FIG. 10. Idem Fig. 9 for $R_c = 4.5 \times 10^7$, 5.5×10^7, 1.0×10^8, 1.5×10^8, 5.0×10^8, 6.0×10^8. In all cases, $E = 10^{-3}$, $\tau = 0.1$, and critical values $R_e = (R_e^7)_c$.

plots are confined to the inner boundary, and spiral anticlockwise. The main difference with respect to Fig. 6 are the contour plots of $|\mathbf{v}|^2$, whose vertical span is now of the order of the diameter of the inner sphere (notice the white spot in the meridional section near the inner boundary) not that of a column (see the white vertical strip in Fig. 6). In the meridional sections of these figures, we have included the contour lines to appreciate the differences. The critical modes for $\tau = 0.1$ and 0.8 have similar behavior. This strongly radially and axially localized thermal convection remind that described in Ref. 28, where the axial structure of the eigenmodes is analyzed by considering a continuously varying density stratification of a pure fluid, unstable near the inner boundary and stable in the outer. For this range of parameters, we have checked that the asymptotic dependence of the neutral stability curves shown in Figs. 11(a) and 11(b) do not vary appreciably when, in addition

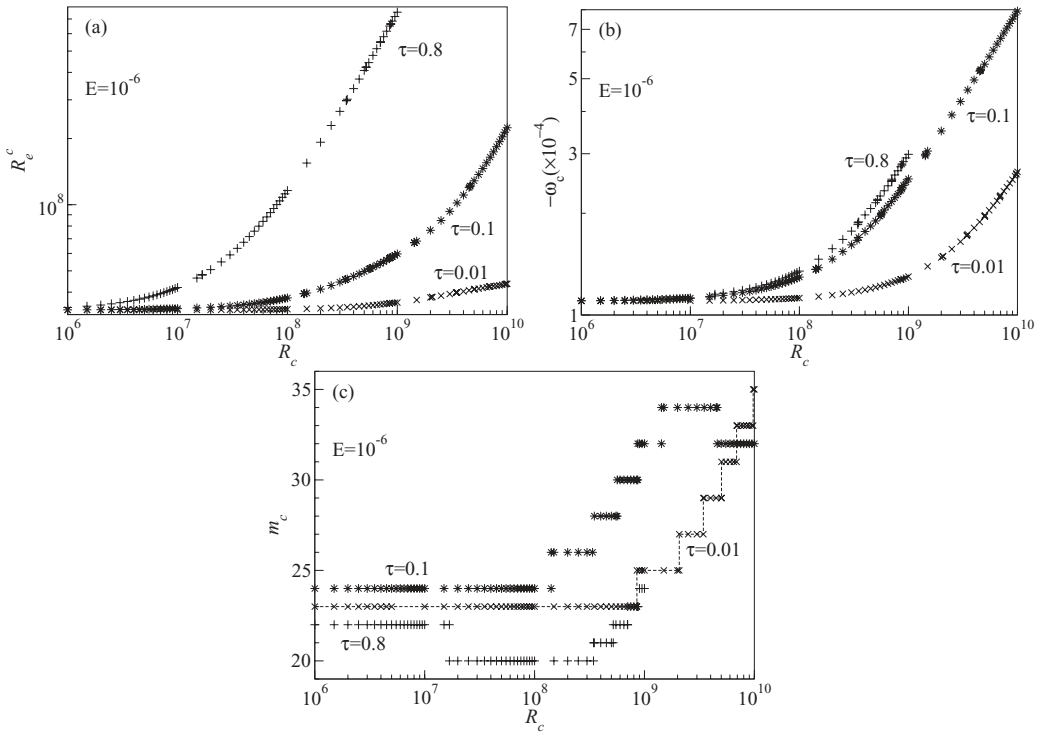

FIG. 11. (a) The critical Rayleigh number R_e^c, (b) the critical precession frequency $-\omega_c$, and (c) the critical wave number m_c for $\tau = 0.01$, $m_c + 1$ for $\tau = 0.1$, and $m_c - 1$ for $\tau = 0.8$, plotted versus R_c for $E = 10^{-6}$.

to the compositional gradient, the Soret effect is included in the model. The separation ratio $S = -0.1$ for $\tau = 0.1$ and 0.8 and $E = 10^{-6}$ was used in the calculations. The crossings of modes do not take place at the same points, but the patterns of convection and the powers of the power laws are those shown in this section. So the changes can be considered as second order effects.

According to Ref. 12 the action of slowly diffusing light material is independent of the sign of R_c provided that $|R_c^{Bu}| \ll \eta^{*2}\sigma$. From our results, we know this is true when the effect of the compositional gradient does not exceed that of the thermal by a large amount. By using, as before, the dimensions of the Earth's outer core, the estimated relation between the parameters, and the values of Figs. 5 and 11, the above condition gives $R_c \ll 2 \times 10^{10}$ for $\tau = 0.1$ and $R_c \ll 2 \times 10^{11}$ for $\tau = 0.01$, which do not contradict the numerical results but neither give an accurate bound for the onset of convection driven by the composition. The same happens with the drift of the waves and wave number of the critical modes. The order of magnitude of $|\omega_c|$ agrees well with our results (taking into consideration that we are comparing different geometries) but, in contrast, we always find prograde drifts.

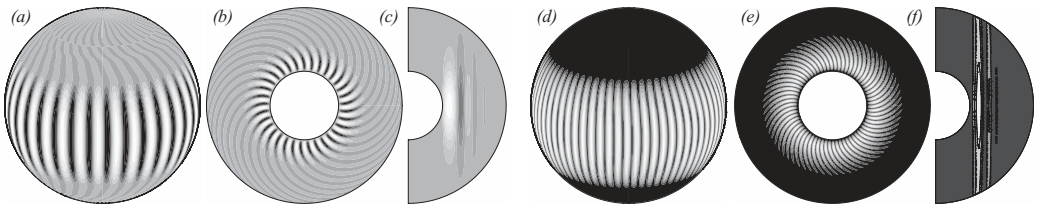

FIG. 12. (a)–(c) Contour plots of critical mode of Θ, and (d)–(f) of $|\mathbf{v}|^2$ for $E = 10^{-6}$, $R_c = 8. \times 10^9$, $\tau = 0.01$, and $m_c = 33$.

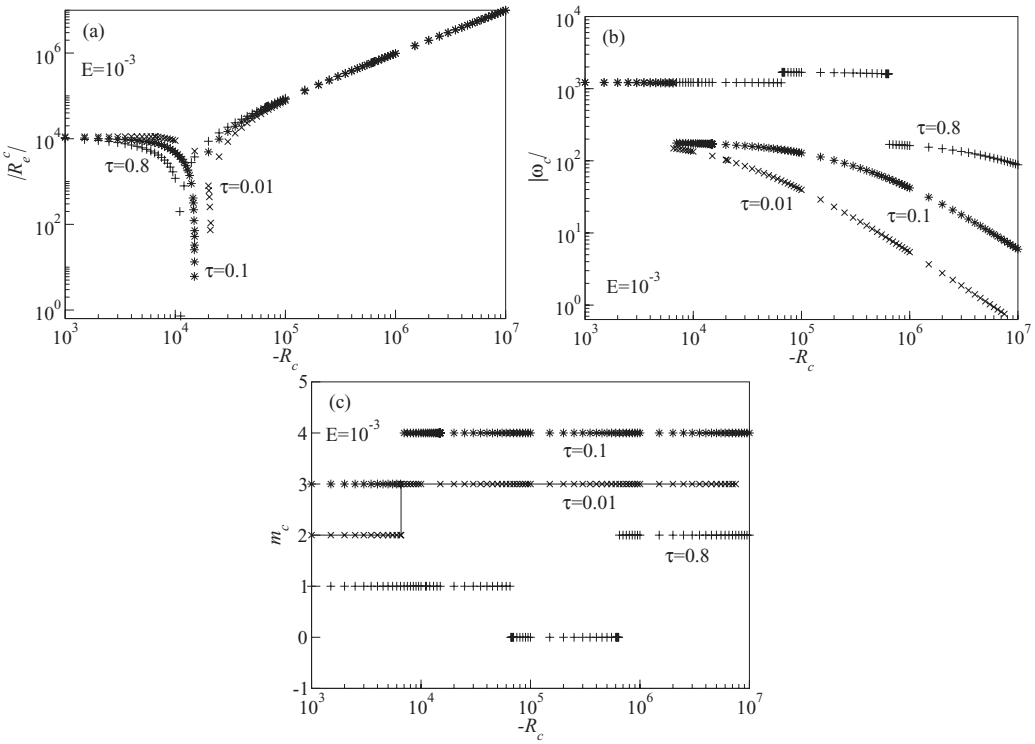

FIG. 13. Absolute value of (a) the critical Rayleigh number R_e^c, (b) the critical precession frequency ω_c, and (c) the critical wave number m_c for $\tau = 0.01$, $m_c + 1$ for $\tau = 0.1$, and $m_c - 1$ for $\tau = 0.8$, plotted versus $-R_c$ for $E = 10^{-3}$.

V. PRANDTL NUMBER $\sigma = 0.001$

A. Positive compositional gradients

For $E = 10^{-3}$ and neglecting the Soret effect, the critical Rayleigh number for a pure fluid of $\sigma = 0.001$ is $R_e^c = 1.108 \times 10^4$ with critical precession frequency $\omega_c = 1.222 \times 10^3$. Notice that in this case $\omega_c > 0$, i.e., a wave of critical wave number $m_c = 2$ drifts in the retrograde direction, although we have checked that this is due to the relatively high E value used for these computations not to the very low σ value.

For this very low σ, the qualitative behavior of the neutral curves, corresponding to different wave numbers m, is not very different from that of Fig. 1(a). The critical Rayleigh numbers $(R_e^m)_c$ are almost independent of m and τ in the interval of R_c computed. As for $\sigma = 0.1$, $(R_e^m)_c$ changes from positive to negative values.

The linear stability analysis of Eqs. (19)–(22) with boundary conditions (23) for $E = 10^{-3}$, $\tau = 0.01$, 0.1, and 0.8 is summarized in Fig. 13. The change of sign corresponds to the descend of the curves in Fig. 13(a). At high $-R_c$, the dependence of the critical Rayleigh number is also almost linear, specifically $R_e^c = -0.81(-R_c)^{1.01}$ and $m_c = 3$ for any τ (see Fig 13(c)). At low $-R_c$, it tends to $R_e^c = 1.1085 \times 10^4$, the critical value of $R_c = 0$. Figure 13(b) shows the dependence of ω_c with $-R_c$. The fast inertial mode is superseded by the compositional slow mode, of prograde drifting, as soon as the compositional gradient becomes relevant. The precession frequencies tend to zero slower than for $\sigma = 0.1$, but the almost hyperbolic dependence of ω_c with $-R_c$ is maintained. In the range computed, we have found $\omega_c = -1.49(-R_c)^{-0.91}$ for $\tau = 0.1$ and $\omega_c = -3.06 \times 10^6(-R_c)^{-0.96}$ for $\tau = 0.01$. The jump to the slow modes is delayed for large τ values.

The preferred mode of convection for low $-R_c$ (close to 10^3), and the three τ computed, corresponds to that of Fig. 14, and except for the concentration is like that obtained for the pure fluid (not shown). The main difference is the new relative maxima of the kinetic energy density which appear at mid-latitudes as $-R_c$ increases. The phase difference between Θ and Σ depends on τ, and

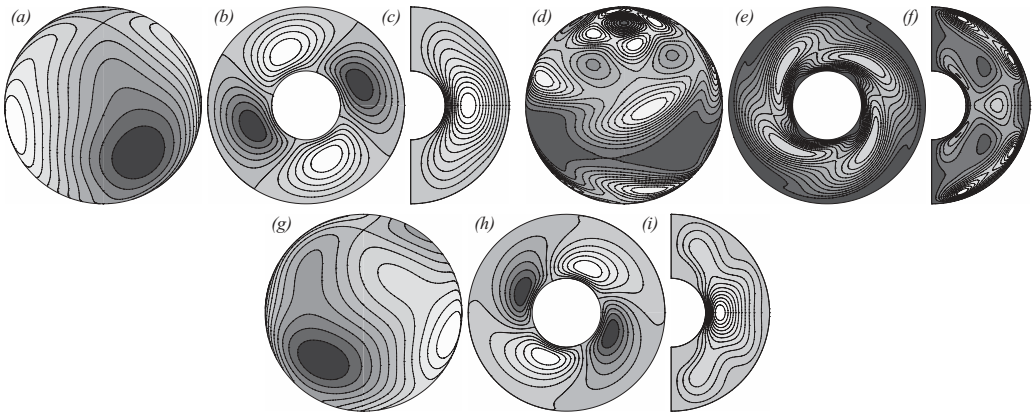

FIG. 14. Idem Fig. 3 for $E = 10^{-3}$, $R_c = -1.0 \times 10^3$, $\tau = 0.01$, and $m_c = 2$.

becomes lower as $-R_c$ increases. In contrast, in the $-R_c \to \infty$ limit the critical mode is like that of Fig. 4 with Θ and Σ in phase because then the simplified equations are (26) and (27). For $\tau = 0.8$, and $6.6 \times 10^4 \lesssim -R_c \lesssim 6.1 \times 10^5$, an antisymmetric eigenfunction of $m_c = 1$, which fills the shell and has polar energy, is preferred.

B. Negative compositional gradients

The results corresponding to the onset of convection for stabilizing compositional gradients, $\tau = 0.01$, 0.1, and 0.8, and $E = 10^{-3}$ are shown in Fig. 15.

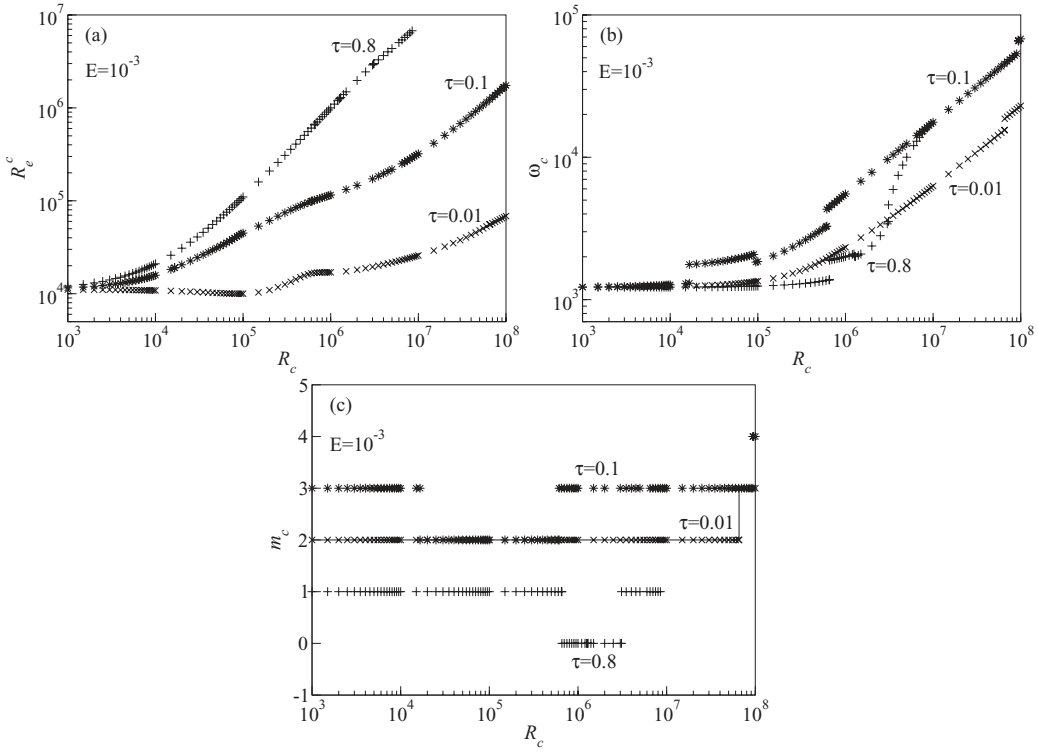

FIG. 15. Value of (a) the critical Rayleigh number R_e^c, (b) the critical precession frequency ω_c, and (c) the critical wave number m_c for $\tau = 0.01$, $m_c + 1$ for $\tau = 0.1$, and $m_c - 1$ for $\tau = 0.8$, plotted versus R_c for $E = 10^{-3}$.

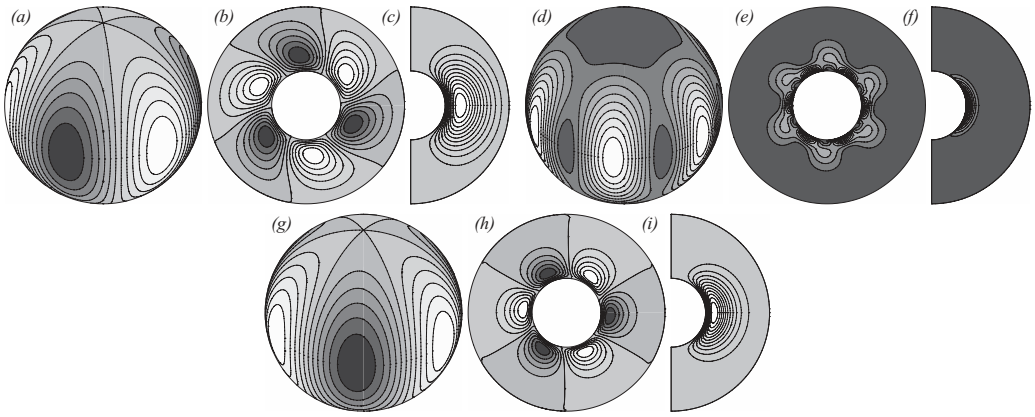

FIG. 16. Idem Fig. 3 for $E = 10^{-3}$, $R_c = 8.5 \times 10^7$, $\tau = 0.01$, and $m_c = 3$.

As in the preceding case, the effect of τ on the onset of convection becomes apparent at lower compositional gradients than for $\sigma = 0.1$ as can be seen comparing Fig. 15(a) with Fig. 7(a), but, in contrast, a higher R_c is needed to get the asymptotic regime. From the estimations of the power laws by considering $R_c > 3 \times 10^7$, it is found that $R_e^c = 5.68 \times 10^{0.51}$ for $\tau = 0.01$, while $R_e^c = 0.86 \times 10^{0.79}$ for $\tau = 0.1$, which could indicate that the high R_c limit for R_e^c is not yet reached at $R_c = 10^8$. On the other hand, ω_c has the same power dependence as that found in Fig. 7(b) for $\sigma = 0.1$, namely, $\omega_c = 1.40 \times 10^{0.52}$ for $\tau = 0.01$, and $\omega_c = 4.11 \times 10^{0.52}$ for $\tau = 0.1$. It is important to realize that with $E = 10^{-3}$, $\omega_c > 0$ for any value of $R_c > 0$, as for the pure fluid. We think this fact is a consequence of the moderate value of E and that the precession frequency would be prograde for a lower E value.

As can be seen in Fig. 15(c), the critical wave number starts to increase only at the end of the interval, and it is always kept much lower than for higher σ values. The first change in the slope of ω_c with $\tau = 0.8$ at $R_c \approx 1.25 \times 10^6$ is due to a change from an antisymmetric to a symmetric mode of convection, although it is not reflected in Fig. 15(c) because the change takes place keeping $m_c = 1$. The abrupt jump at $R_c = 3.10 \times 10^6$ is connected with an interchange from $m_c = 1$ to $m_c = 2$ symmetric modes.

As for $\sigma = 0.1$, the type of preferred modes at low R_c is independent of τ, and it is like that of Fig. 14. The differences among the contour plots of Θ and Σ depend on τ. For $\tau = 0.01$, there is a continuous transition between the initial mode of convection and that preferred at high R_c. The latter is shown in Fig. 16 at $R_c = 8.5 \times 10^7$ and for $m_c = 3$. Following the preferred eigenfunctions on the corresponding curve ($\times$ in Fig. 15) from $R_c = 10^3$ up to higher values, we have seen that the mid-latitude external maxima of the kinetic energy density weaken and disappear. After, for $R_c > 10^5$, the contour plots of the kinetic energy start to develop an internal relative maxima near the inner sphere in the vertical of those external, and at higher R_c the remaining high latitude external vortices also disappear and the inner are reinforced. Finally, these latter increase their size and collapse, giving rise to the very localized contour plots of Figs. 16(d)–16(f) but with $m_c = 2$. The $m_c = 3$ modes, preferred at the end of the interval, belong to the same family of solutions.

Figure 17 shows two preferred modes of convection in the intermediate range of R_c for $\tau = 0.1$. For every solution, the contour plots of Σ are very similar to those of Θ with phase differences that never exceed $\pi/2m$. When the effect of the concentration gradient starts to be important the patterns of convection are first antisymmetric and after symmetric, but in both cases the kinetic energy density is concentrated at the poles. In the high R_c limit, the eigenmodes are like those of Fig. 16 (but for m_c) for any τ computed. Despite the strong change of the slope of the curve (R_c, ω_c) for $\tau = 0.8$ in Fig. 15(b), in the range $6.5 \times 10^5 < R_c < 3.0 \times 10^6$ the preferred patterns of convection are basically those shown in Fig. 17, and after those of the high R_c limit.

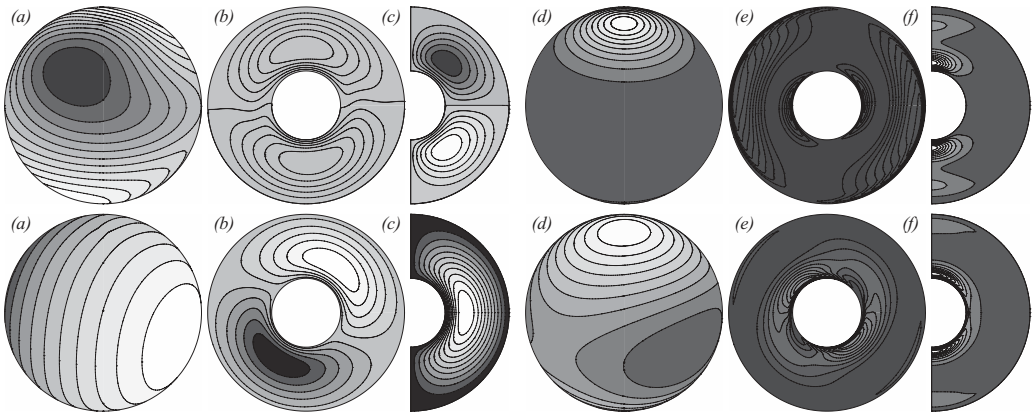

FIG. 17. Idem Fig. 12 for, from top to bottom, $R_c = 6 \times 10^4, 5 \times 10^5$. In both rows, $E = 10^{-3}$, $\tau = 0.1$, $m_c = 1$.

VI. CONCLUSIONS

By comparing the results obtained in this paper with those known for pure fluids we can conclude that:

- In a mixture of fluids of low Prandtl number, the compositional effect starts to be important when $|R_c|$ is approximately of the order of R_e^c. Therefore, when the dynamics of the convection is controlled by the rotation rate, the double-diffusive effects are negligible and the preferred modes of convection are those of the pure fluid. In such a case, one should expect the same dependence of the modes with the type of heating as with $|R_c| = 0$. Moreover, low Ekman numbers require higher $|R_c|$ values to give significant differences with the simple thermal diffusion problem.
- With stabilizing compositional gradients ($C_i > C_o$):

  The onset of thermal convection is delayed, i.e., R_e^c is higher than that obtained for $R_c = 0$. The precession frequency $|\omega_c|$ and m_c also grow. For $\sigma = 0.1$, the pattern of convection consists of vortices confined near the inner boundary whose vertical extend depends mainly on E and R_c. The effect of increasing R_c, in contrast to that of decreasing E, is to shorten the vertical span of the vortices of $|\mathbf{v}|^2$. So, we can conclude that the thermosolutal convection, driven mainly by compositional gradients, breaks the columnar configuration of the velocity field existing for pure fluids.

  We have not found an asymptotic law between R_c and R_e^c independent of any parameter, but $|\omega_c|$ seems to increase as $R_c^{1/2}$ for any set of parameters employed. It is possible that, in this case, the asymptotic limit has not been reached due to the computational cost.

  The main effect of lowering the Prandtl number to $\sigma = 0.001$ is to reduce the wave number of the patterns of convection, and to change them in the region of parameters where the competition between compositional and thermal gradients is important.

  Moderate-E thermosolutal convection and $\sigma = 0.1$ gives rises to a great variety of patterns of convection. In particular, the tesseral modes (corresponding to dominant spherical harmonics of $l - m \neq 0$) become critical for a fixed m provided the compositional gradient be negative and its influence stronger than that of the temperature gradient.
- With destabilizing compositional gradients ($C_i < C_o$):

  The critical value for the onset of convection R_e^c diminishes, and the drift of the waves slows down. The convection can be triggered even in presence of stabilizing temperature gradients. In addition, the effect of strong compositional gradients is to lower the azimuthal wave number of the preferred modes. As $-R_c$ is increased, $m_c = 3$ becomes preferred for both $E = 10^{-3}$ and $E = 10^{-6}$, recovering the value of very low rotation rates. Then, the patterns of convection are sectorial like those well known for a pure fluid, even when the convection is driven by the compositional gradients. The difference among the eigenfunctions of $m_c = 3$ corresponding to

high and low E comes from the velocity field. At low E, the kinetic energy density is columnar, and at high it is attached to the outer sphere.

The values $E = 10^{-3}$ and 10^{-6}, $\tau = 0.1$, 0.01, and 0.8, and $\sigma = 0.1$ and 0.001 used in the calculations are sufficiently different as to state that the almost linear dependence between R_c and R_e^c and the inversely proportional between R_c and ω_c are independent of E and τ and σ.

The main effect of lowering σ is to anticipate the onset of the compositional convection, and to delay the slowing down of the waves up to high $-R_c$ values.

ACKNOWLEDGMENTS

This work has been supported by Spain MCI (Ministerio de Ciencia e Innovación), and Catalonia AGAUR (Agència de Gestió d'Ajuts Universita-ris ide Recerca) under Grant Nos. MTM2010-16930 and 2009-SGR-67, respectively. We thank E. García-Berro for the useful information on stellar convection supplied.

[1] J. P. Poirier, *Introduction to the Physics of the Earth's Interior*, 2nd ed. (Cambridge University Press, Cambridge, 2000).
[2] D. A. Ostlie and B. W. Carroll, *An Introduction to Modern Stellar Astrophysics* (Addison-Wesley, Boston, 1996).
[3] P. H. Roberts, "On the thermal instability of a rotating fluid sphere containing heat sources," Philos. Trans. R. Soc. London, Ser. A **263**, 93–117 (1968).
[4] F. H. Busse, "Thermal instabilities in rapidly rotating systems," J. Fluid Mech. **44**, 441–460 (1970).
[5] E. Dormy, A. M. Soward, C. A. Jones, D. Jault, and P. Cardin, "The onset of thermal convection in rotating spherical shells," J. Fluid Mech. **501**, 43–70 (2004).
[6] K. Zhang and X. Liao, "A new asymptotic method for the analysis of convection in a rapidly rotating sphere," J. Fluid Mech. **518**, 319–346 (2004).
[7] K. Zhang, X. Liao, and F. H. Busse, "Asymptotic solutions of convection in rapidly rotating non-slip spheres," J. Fluid Mech. **578**, 371–380 (2007).
[8] M. Net, F. Garcia, and J. Sánchez, "On the onset of low-Prandtl-number convection in rotating spherical shells: Non-slip boundary conditions," J. Fluid Mech. **601**, 317–337 (2008).
[9] F. Garcia, J. Sánchez, and M. Net, "Antisymmetric polar modes of thermal convection in rotating spherical fluid shells at high Taylor numbers," Phys. Rev. Lett. **101**, 194501–194504 (2008).
[10] E. Knobloch, "Bifurcations in rotating systems," in *Lectures on Solar and Planetary Dynamos*, Publications of the Newton Institute No. 2, edited by M. R.E. Proctor, and A. D. Gilbert (Cambridge University Press, Cambridge, 1994).
[11] K. Zhang, "On coupling between the Poincaré equation and the heat equation: Non-slip boundary condition," J. Fluid Mech. **284**, 239–256 (1995).
[12] F. H. Busse, "Is low Rayleigh number convection possible in the Earth's core?" Geophys. Res. Lett. **29**, 1105, doi:10.1029/2001GL014597 (2002).
[13] S. V. Starchenko, M. S. Kotelnikova, and I. V. Maslov, "Marginal stability of almost adiabatic planetary convection," Geophys. Astrophys. Fluid Dyn. **100**, 397–427 (2006).
[14] E. A. Spiegel and G. Veronis, "On the Boussinesq approximation for a compressible fluid," Astrophys. J. **131**, 442–447 (1960).
[15] J. R. Lister and B. A. Buffet, "The strength and efficiency of thermal and compositional convection in the Earth's core," Phys. Earth Planet. Inter. **91**, 17–30 (1995).
[16] S. I. Braginsky, "Towards a realistic theory of geodynamo," Geophys. Astrophys. Fluid Dyn. **60**, 89–134 (1991).
[17] G. A. Glatzmaier and P. H. Roberts, "An anelastic evolutionary geodynamo simulation driven by compositional and thermal convection," Physica D **97**, 81–94 (1996).
[18] M. Breuer, A. Manglik, J. Wicht, T. Trümper, H. Harder, and U. Hansen, "Thermochemically driven convection in a rotating spherical shell," Geophys. J. Int. **183**, 150–162 (2010).
[19] A. Manglik, J. Wicht, and U. R. Christensen, "A dynamo model with double diffusive convection for Mercury's core," Earth Planet. Sci. Lett. **289**, 619–628 (2010).
[20] D. Gubbins, T. G. Masters, and J. A. Jacobs, "Thermal evolution of the Earth's core," Geophys. J. R. Astron. Soc. **59**, 57–99 (1979).
[21] D. E. Loper and P. H. Roberts, "Compositional convection and the gravitationally powered dynamo," in *Stellar and Planetary Magnetism*, edited by A. M. Soward (Gordon and Breach, New York, 1983), pp. 297–327.
[22] G. A. de Wijs, G. Kresse, L. Vočadlo, D. Dobson, D. Alfè, M. J. Gillan, and G. D. Price, "The viscosity of liquid iron at the physical conditions of the Earth's core," Nature (London) **392**, 805–807 (1998).
[23] S. R. de Groot and P. Mazur, *Non-Equilibrium Thermodynamics* (Dover, Amsterdam, 1962).
[24] L. D. Landau and E. M. Lifshitz, *Fluid Mechanics* (Pergamon, Oxford, 1975).
[25] W. Hort, S. J. Linz, and M. Lücke, "Onset of convection in binary gas mixtures: Role of the Dufour effect," Phys. Rev. A **45**, 3737–3747 (1992).
[26] A. Alonso, M. Net, I. Mercader, and E. Knobloch, "Onset of convection in a rotating annulus with radial gravity and heating," Fluid Dyn. Res. **24**, 133–145 (1999).
[27] Z. Dai, K. Zhang, G. Schubert, and X. Liao, "Simulations of nonlinear pore-water convection in spherical shells," Phys. Fluids **20**, 026601 (2008).
[28] A. P. Bassom, A. M. Soward, and S. V. Starchenko, "The onset of strongly localized thermal convection in rotating spherical shells," J. Fluid Mech. **689**, 376–416 (2011).